Tracking the interfacial charge transfer behavior of hydrothermally synthesized ZnO nanostructures via complementary electrogravimetric methods

Wanli Gao, Hubert Perrot, Ozlem Sel

Tracking interfacial charge transfer behavior of hydrothermally synthesized ZnO nanostructures via complementary electrogravimetric methods

Wanli Gao,[a] Hubert Perrot *[a] and Ozlem Sel*[a]

[a.] Sorbonne Université, LISE, CNRS, UMR 8235, LISE, F-75005, Paris, France.

Abstract:

The mechanism of species fluxes during charge-discharge process in nanostructured ZnO electrode was studied by a combined methodology of electrochemical quartz-crystal microbalance (EQCM) and *ac*-electrogravimetry. Under the conditions of this study, anions (SO_4^{2-}) possess the highest kinetics to be transferred at the electrode/electrolyte interface in charge balance while cations (identified as $Na^+.5H_2O$ and Na^+) play the major part as charge carriers. Free H_2O molecules present a sluggish behavior and their interfacial transfer occurs at low scan rate or low frequencies. These findings shed light on the nature of ions and solvent participation in charge balance of hydrothermally synthesized ZnO nanostructures directly grown on the QCM device. The combined methodology proposed herein provides dynamic and gravimetric analysis of interfacial charge transfer and can be extended to investigate other nanostructured metal oxide-based electrodes for energy storage.

Keywords: Zinc oxide, Supercapacitor, EQCM, *Ac*-electrogravimetry, Ionic transfer dynamics

Introduction

Supercapacitors (SCs) are a class of electrochemical energy storage devices well suited to the rapid storage and release of energy.[1] The last four decades have seen a tremendous burgeoning of scientific and industrial interest into the potential applications of SCs, mainly due to their high power density and long cycle life.[2, 3] Numerous research efforts have been dedicated to investigating the electrode materials, which play an essential role in optimizing the electrochemical performance of SCs.

Transition metal oxides have been intensively studied as electrode materials due to their fast and reversible redox reactions occurring at or near the electrode surface, which can provide significantly higher capacitances.[4-7] Generally, metal oxides can offer higher energy density than conventional carbon materials and better electrochemical stability than conducting polymers.[2] To date, transitional metal oxides, such as ruthenium oxide (RuO_2),[8] manganese dioxide (MnO_2),[9] zinc oxide (ZnO)[10] and nickel oxide (NiO)[11] have been intensively studied as electrode materials, which can offer additional pseudocapacitances during electrochemical performance.

Among these candidates, ZnO nanomaterials have been widely used due to its low cost, easy fabrication, morphological diversity and electrochemical activities.[12-15] ZnO nanomaterials can be solely deposited on the substrate[10] or composited with other metal oxides,[14] conducting polymers[16] and carbon-based materials[17] to serve as energy storage electrodes. However, of great fundamental importance but almost barely touched is the mechanism of ionic/non-ionic fluxes during charge-discharge process in

ZnO-based electrodes, which plays an essential role in the design of supercapacitor electrodes with high efficiency.

Electrochemical quartz-crystal microbalance (EQCM) has gained wide applicability to evaluate the electrochemical behaviour of electrodes,[18-22] particularly *in situ* capturing of the global transfer of the species at the electrode/electrolyte interface. Mass and charge variations measured simultaneously during the electrode cycling allow the derivation of the global mass per mole of electrons (MPE) that is exchanged between the electrode and the electrolyte according to the equation:

$$MPE = F\frac{\Delta m}{\Delta q} = F\frac{\Delta m/\Delta t}{\Delta q/\Delta t} = F\frac{\Delta m/\Delta t}{I}$$

with F is the Faraday number, Δm and Δq are the mass and charge variations, respectively. If only one species is exchanged, then the MPE corresponds to its molar mass. In the cases where multiple ion transfer occurs, using Faraday's law to interpret classical EQCM data reaches its limitations. To discriminate between the involved species, Donnan-type electrical double layer models were incorporated into the gravimetric EQCM equations.[23] Besides, the complex character of the electrode mass changes as well as the quantification of viscoelastic properties of the electrodes (and also possibly formed solid electrolyte interface (SEI) layer) can be investigated using multiharmonic EQCM with dissipation monitoring (EQCM-D).[24]

Additionally, it has been demonstrated that coupling the QCM with electrochemical impedance spectroscopy (the so-called *ac*-electrogravimetry) contributes to disentangle the subtleties of global charge compensation process involving multiple

species, offering a quantitative picture of each participant with their transfer kinetics and identifying them by their molar masses.

The *ac*-electrogravimetric measurements can detect interfacial processes occurring in the frequency range from ~ 100 Hz to as low as ~ 1 mHz, and separates multi-species contribution with different kinetics, reaching a higher selectivity than slow scan-rate cyclic voltammetry.[25]

In *ac*-electrogravimetry, under a fixed potential with a small sinusoidal perturbation, frequency dependant mass and charge variations are obtained and used to generate both the classical EIS transfer function (TF), $\Delta E/\Delta I(\omega)$ and the mass/potential TF, $\Delta m/\Delta E(\omega)$. These TFs are then fitted with an appropriate model to obtain detailed identification of the species involved in the charge transfer mechanism, along with the kinetics and the relative concentrations associated with each species.[26]

In the present work, this non-classical but emerging methodology in the energy storage domain[27-29] is adopted to characterize the electrochemical energy storage behaviour of ZnO-based electrodes and elucidate the subtleties in transfer of species during charge balance. To the best of our knowledge, this is the first time that ZnO is grown on QCM devices for energy storage purposes and investigated by the classical EQCM and its complementary counterpart *ac*-electrogravimetry for understanding its charge storage mechanism.

Experimental

A precursor solution was prepared with 0.02 M zinc nitrate hexahydrate and 0.02 M hexamethylenetetramine (HMTA). A quartz resonator (9 MHz-AWS, Valencia, Spain) was immersed in the solution, which was transferred to a Teflon-lined stainless steel autoclave and maintained at 120 °C for 12 h. The resonator is placed at the bottom of the autoclave. By this way, the back side is protected and only the upper side of the crystal was found to be deposited with ZnO nanostructures. After the hydrothermal process, ZnO nanostructures generated on the resonators were rinsed several times with deionized water.

EQCM and *ac*-electrogravimetry measurements were performed in 0.25 M Na_2SO_4 under nitrogen atmosphere. ZnO nanostructures grown on the quartz resonator were used as the working electrode, with Ag/AgCl (3 M KCl saturated with AgCl) and platinum gauze as the reference and counter electrode, respectively. The potential window for EQCM was confined between 0 V and 0.6 V vs. Ag/AgCl in cyclic voltammetry (CV) (the OCV was at 0.15 V vs. Ag/AgCl) and 0 V and 0.8 V vs. Ag/AgCl in galvanostatic charge/discharge (GCD). A lab-made QCM device (Miller oscillator) was used to measure frequency shift (Δf) of the quartz crystals. The mass change (Δm) of ZnO electrode on the quartz crystals during electrochemical process can be estimated by the microbalance frequency shift (Δf) through Sauerbrey equation,[30] i.e., $\Delta f = -C_f \times \Delta m$, where C_f is the experimental sensitivity factor of the quartz crystal resonator ($C_f = 16.3\times10^7$ Hz.g^{-1}.cm^2). The details of the estimation of the experimental sensitivity factor are previously given.[31]

For *ac*-electrogravimetry measurements, a four-channel frequency response analyzer (FRA, Solartron 1254) and a lab- made potentiostat (SOTELEM-PGSTAT) were used. The QCM was performed under dynamic regime, and the modified working electrode was polarized at selected potentials to which a sinusoidal small amplitude potential perturbation was superimposed. The frequency range was between 63 KHz and 10 mHz. The mass change, Δ*m*, of the working electrode was measured simultaneously with the *ac* response, Δ*I*, of the electrochemical system. Frequency/voltage converter is the key **c**omponent of the *ac*-electrogravimetry set-up which translates the QCM frequency response (Δ*f*) to a continuous voltage change (ΔV_f) with the aim of obtaining a transfer function (TF) via a frequency response analyzer (FRA) (which cannot directly analyze the frequency response). Finally, the resulting signals $\Delta V_f/\Delta V(\omega)$ and $\Delta V/\Delta I(\omega)$ were sent to a four-channel FRA, which led to the electrogravimetric TF ($\Delta m/\Delta E(\omega)$) and the electrical TF ($\Delta E/\Delta I(\omega)$) to be obtained simultaneously at a given potential and frequency modulation, *f* (pulsation, $\omega=2\pi f$).

Theoretical Part

Under the effect of a sinusoidal potential perturbation with low amplitude, ΔE, imposed to the electrode/film/electrolyte system, sinusoidal fluctuations of concentration, ΔC_i are observed. The theoretical TFs are calculated through the following equations:[28, 32]

$$\frac{\Delta C}{\Delta E}(\omega) = \left(\frac{-G_i}{\mathrm{j}\omega d_f + K_i}\right) \qquad \textbf{(eq. 1)}$$

$$\frac{\Delta E}{\Delta I}(\omega) = \left(\frac{1}{\mathrm{j}\omega F d_f \sum \frac{G_i}{\mathrm{j}\omega d_f + K_i}}\right) \qquad \textbf{(eq. 2)}$$

$$\frac{\Delta q}{\Delta E}(\omega) = \mathrm{F} \cdot d_f \left(\sum \frac{G_i}{\mathrm{j}\omega d_f + K_i}\right) \qquad \textbf{(eq. 3)}$$

$$\frac{\Delta m}{\Delta E}(\omega) = -d_f \left(\sum M_i \frac{G_i}{\mathrm{j}\omega d_f + K_i} \right) \qquad \textbf{(eq. 4)}$$

where ΔC_i presents concentration variation for each species, $\boldsymbol{\omega}$ is the pulsation, d_f is the film thickness, M_i depicts the molar mass of involved species, K_i and G_i are the partial derivatives of the flux (J_i) with respect to the concentration and the potential, respectively. K_i represents the transfer kinetics of each species while G_i is the reciprocal of the transfer resistance (Rt_i=1/FG_i), exhibiting the ease or difficulty in the species transfer at the film/electrolyte interface (*i:* ions for **eq. 1-3**, and *i:* ions and non-charged species for **eq. 4**).

The theoretical expressions (**eq. 2-4**) were used to fit the experimental responses of the electrochemical impedance, $\Delta E/\Delta I(\omega)$, the charge/potential TF, $\Delta q/\Delta E(\omega)$ and the electrogravimetric TF, $\Delta m/\Delta E(\omega)$, which provided the key parameters (M_i, K_i and G_i) related to each species (where *i* can be a cation, an anion or solvent) to be extracted. With the same set of parameters, all the TFs including cross and partial TFs (detailed in Ref.26-29) were fitted where a good agreement between the experimental and the theoretical functions in terms of both the shape and the frequencies should be achieved, to consider that these parameters (M_i, K_i and G_i) are unique.

Results and Discussion

The synthesis of the nanostructures were performed directly on the quartz resonators by hydrothermal method. As shown in **Fig. 1a**, ZnO nanostructures are densely grown on the quartz resonator, formed by flower-like bundles of individual nanorods with a diameter of ~300-800 nm and length of ~2-7 µm. The discrete ZnO nanorods may facilitate the exposure to the electrolyte and thus offer a large surface area for the electrochemical processes. XRD patterns are recorded (**Fig. 1b**) and the peaks present between 32° and 69° demonstrate that the synthesized ZnO nanorods exhibit the crystalline nature of wurtzite hexagonal structure, which is in good agreement with standard ZnO peaks (JCPDS 36-1451). [33, 34]

Cyclic Electrogravimetry (EQCM) and QCM-coupled GCD: The electrochemical performance of ZnO nanorods was characterized by cyclic voltammetry (CV) and galvonastatic charge-discharge (GCD) techniques. The QCM was coupled with both measurements to track the simultaneous frequency shifts of the ZnO-based electrode during cycling, which can be converted into mass responses through Sauerbrey equation.[30] **Fig. 2a** exhibits approximately rectangular CV curves, with a slight contribution of a cathodic peak around 0.1 V and an anodic peak around 0.2 V.

This electrochemical behaviour due to the dominant capacitive response in the CV curve can be attributed to an electroadsorption process of Na^+ ions occurring at different electroactive sites of the ZnO electrode:

$$ZnO + Na^+ + e^- \leftrightarrow (ZnO)^-_{surface}\ Na^+$$

However, this simplified scheme does not take into account of (i) the ion solvation effect, (ii) the possible presence of more than one ionic species which may participate in the charge

compensation process and affect the charge/discharge rates, and (iii) the influence of free electrolyte molecules that can interact, indirectly, with the electrodes.

Utilizing the simultaneous QCM measurements permits the corresponding mass responses (Δm-E) to be obtained during CV scans (**Fig. 2b**). Mass response mainly presents ingress/egress during cathodic/anodic sweep, which is indicative of cation participation in charge compensation process.[32] GCD curves were measured to further evaluate the electrochemical performance of ZnO-based electrode.

The corresponding mass-time response proceeds in an inverse pace with potential-time response, i.e., mass decrease during charging and mass increase during discharging, which indicates that the cation plays a major role in charge balance.

To obtain indications on the nature of the transferred species, the $MPE=F\Delta m/\Delta q$ was calculated from the EQCM data (**Fig. S1**, Supporting information). If only one species is exchanged, then the MPE corresponds to its molar mass. Positive and negative values of the MPE correspond to a major contribution to the energy storage mechanism by anions and cations, respectively. Here, we obtain a MPE of ~-100 $g.mol^{-1}$ below 0.3 V and ~-50 $g.mol^{-1}$ above 0.4 V for the cathodic sweep and anodic sweep, respectively. The higher values for the cathodic sweep suggest that the cations are hydrated and/or accompanied by free solvent molecules. This value lowers during the anodic sweep (~-50 $g.mol^{-1}$), indicating that multiple species are exchanged and interfacial behaviour is complex.

QCM-coupled CV and GCD measurements are performed at a certain scan rate or current density, therefore they require either the incorporation of Donnan-type models into the gravimetric EQCM equations[23] or complementary methods to elucidate if there is a multiple species contribution to the charge compensation process.[35] To get a deeper insight into the

charge compensation behaviour occurring in the ZnO-based electrode, from both gravimetrical and kinetic point of view, the *ac*-electrogravimetry was suggested. The different scenarios of the charge compensation process for ZnO-based electrodes are scrutinized by this coupled method emerging in the field of energy storage.[27, 29]

QCM-coupled to Electrochemical Impedance (*Ac*-electrogravimetry): *Ac*-electrogravimetry measurements were performed in the same potential range used for CV measurements, at various states-of-polarization from 0 V to 0.6V vs. Ag/AgCl with an interval of 100 mV. **Fig. 3a** and **b** present $\Delta q/\Delta E(\omega)$ (calculated from the electrochemical impedance, theoretical part in **eq. 2** and **3**) and $\Delta m/\Delta E(\omega)$ TFs at 0.3V, where the experimental data were fitted using theoretical functions in eq. 3 and 4. It is important to note that for the $\Delta m/\Delta E(\omega)$ TF, the experimental data were not visualized at high frequency region in **Fig. 3b** beyond ~ 100 Hz due to the instrumental limitations, i.e., the validity region of the frequency-voltage convertor is ~100 Hz to ~ 1 mHz. This may indicate that there is a fast species contributing to the charge storage but cannot be detected by *ac*-electrogravimetry with the current frequency-voltage convertor. Theoretically, anions and cations share the same response behaviour in $\Delta q/\Delta E(\omega)$ TF, but anions characteristically appear in the quadrant I (Cartesian system) in $\Delta m/\Delta E(\omega)$ while cations locate in the quadrant III, as shown in **Fig. 3c** and **d**. Therefore, in the present work, the mass response at high frequency emerging in the quadrant I can originate from either anions or free H_2O molecules with the same transfer direction as anions.[26] Herein, four species based on different kinetics, i.e., anions (SO_4^{2-}), hydrated cations ($Na^+.5H_2O$), cations (Na^+) and H_2O molecules were proposed which led to a good agreement between the experimental and the theoretical functions in terms of both the shape and the frequencies (**Fig. 3**). It is highlighted that the identification of the species can be achieved thanks to the

electrogravimetric TF ($\Delta m/\Delta E(\omega)$) which involves the molar mass (M_i) of the species involved in the charge compensations (**eq. 4**). This configuration was also verified by the so-called partial TFs (obtained by removing the contribution of one of the species contribution, and analysing the residual response) (not shown).

Then, the *ac*-electrogravimetry data obtained at various states-of-polarization from 0 V to 0.6V vs. Ag/AgCl were analysed and it was observed that the presence of several species persists. This finding is further supported by comparing the *ac*-electrogravimetry data with that of EQCM (see the section: *Comparison of the EQCM and Ac-electrogravimerty mass responses*).

The transfer kinetics of each species, K_i, are summarized in **Fig. 4a**. SO_4^{2-} anions exhibit the highest kinetics of transfer at the electrode/electrolyte interface in the charge compensation process, followed by hydrated cations ($Na^+.5H_2O$) and dehydrated cations (Na^+), and H_2O molecules present the lowest kinetics, i.e., K (SO_4^{2-}) > K ($Na^+.5H_2O$) > K (Na^+)> K (H_2O). It is in good agreement with the inverse order of their transfer resistances: R_t (SO_4^{2-}) < R_t ($Na^+.5H_2O$) < R_t (Na^+) < R_t (H_2O), as depicted in **Fig. 4b**. The contribution of various species to electrochemical reactions with different kinetics of transfer has already been observed in the earlier work of Hillman *et al.* on nickel hydroxide thin films by combining probe beam deflection (PBD) technique and EQCM,[36-38] and also in our recent work on SWCNT based electrodes.[27]

The charge storage mechanism of another transitional metal oxide, MnO_2, has been widely investigated, and it was proposed that the charge could be stored by either i) the surface adsorption of alkali metal cations (C^+)[39] or ii) the intercalation of both protons (H^+) and alkali metal cations (C^+)[40, 41] in the electrolyte. However, direct analogy of the charge storage

mechanism proposed for the other metal oxides may not be applicable to ZnO. In the present work, SO_4^{2-} and $Na^+.5H_2O$ present a quick response upon potential perturbation, which is presumably ascribed to their fast electroadsorption behaviour. Dehydrated Na^+ is also considered to be electroadsorbed but in the ZnO bulk, on to the less accessible sites, due to a relatively slow transfer kinetics (**Fig. 5**). Furthermore, free H_2O molecule exhibits a sluggish behaviour and participates in charge balance at lowest frequencies. It is supposed to be electrodragged by Na^+,[27] as evidenced by the same flux direction of H_2O and Na^+.

Actually, it is speculated that there exist at least two different electroactive sites for charge storage in synthesized ZnO nanostructures. The first is on the surface of ZnO, where the charge storage occurs (under the conditions of this study) either by the electroadsorption and electrodesorption of SO_4^{2-} and $Na^+.5H_2O$, respectively (**Fig. 5**). After the surficial electroactive sites are saturated with SO_4^{2-} and $Na^+.5H_2O$ by a fast electroadsorption behaviour, contributing to the responses at high frequency (HF) in *ac*-electrogravimetry (Fig. 3b), the second electroactive sites in the bulk of ZnO may begin to come into use. Dehydrated $Na^+.5H_2O$ (i.e., Na^+) may electrodrag free H_2O molecules into/out of ZnO bulk and, consequently, bring about a response from free H_2O molecules at lowest frequency (LF) in *ac*-electrogravimetry (Fig. 3b).

Comparison of the EQCM and *Ac*-electrogravimerty mass responses: In order to validate our hypothesis involving multi-species contribution to the charge storage and also to confirm the presence of the anionic species appearing at the HF region (see theoretical curve in **Fig. 3b**), a methodology benefiting from the complementarity of the EQCM and *ac*-electrogravimetry is developed as follows:[27] From *ac*-electrogravimetry, the relative concentration changes of each species (ΔC_i) with respect to the potential variation can be estimated by using **eq. 5**;

specifically, the estimation of the relative concentration change with respect to the individual species ($\boldsymbol{C_i - C_0}$) can be obtained after integration of **eq. 5**:

$$\left.\frac{\Delta C}{\Delta E}\right)_{\omega \to 0} = \left(\frac{-G_i}{K_i}\right) \qquad \textbf{(eq. 5)}$$

The concentration variation of individual species ($\boldsymbol{C_i - C_0}$) obtained from *ac*-electrogravimetry is shown in **Fig. 6a**. These $\boldsymbol{C_i - C_0}$ values are transformed into corresponding mass variations of each species (**Fig. 6b**). Subsequently, the total mass change (total Δ*m* from *ac*-electrogravimetry in **Fig. 6c**) is reconstructed by the addition of individual mass contribution from all species concerned in *ac*-electrogravimetry. A good agreement between the total mass change from *ac*-electrogravimetry and the EQCM response obtained at 10 mV/s emerges. It is further highlighted that *ac*-electrogravimetry results are obtained from individual measurements at stationary potentials and the reconstructed mass response is in good agreement with the EQCM data from cyclic voltammetry at the lowest scan rate measured. This is highly significant since it evidences that the *ac*-electrogravimetry result in **Fig. 6b** is indeed a deconvolution of the global EQCM mass response into distinct contributions. Furthermore, since free H_2O molecules display the lowest transfer kinetics in charge balance (the slowest species), the partial mass change (partial Δ*m* in **Fig. 6c**) is obtained with the removal of the mass contributions from free H_2O molecules. It presents the mass response at high, intermediate and intermediate-low frequencies. Then, a close agreement between the partial Δ*m* from *ac*-electrogravimetry and EQCM response at a high scan rate (100 mV/s) (**Fig. 6d**) is also achieved. This implies that all of these 4 species detected including the free H_2O molecules can be transferred at the electrode/electrolyte interface at low scan rate (10 mV/s). However, it hardly occurs for H_2O to be transferred at the electrode/electrolyte interface at a higher scan rate (100 mV/s). These comparisons present

further evidence for the fitting hypothesis of the *ac*-electrogravimetry data that the missing responses at HF are from anion contributions. It is evident that if the contribution of the anions is neglected, a good agreement between the EQCM and *ac*-electrogravimetry would not be achieved (**Fig. 6**). These results highlight the complementarity of the EQCM and *ac*-electrogravimetry, the limitations of either of which can be compensated by the other to unveil the subtleties of the charge storage mechanisms.

Conclusions

The complementary combination of EQCM and *ac*-electrogravimetry was proposed herein to study the charge storage mechanism of hydrothermally synthesized ZnO nanostructures. EQCM provides a global mass response from cations in charge storage/delivery process, while *ac*-electrogravimetry offers a gravimetric and dynamic picture on the subtleties during this process: four different species (SO_4^{2-}, $Na^+.5H_2O$, Na^+, and H_2O) were detected to participate in charge balance with different kinetics to transfer the electrode/electrolyte interface. This study further emphasizes the complementarity of the EQCM and *ac*-electrogravimetry where certain instrumental limitations that challenge the detection of fast ion dynamics can be overcome by exploiting the two methods. This combined methodology can be extended to investigate the charge storage mechanism and species fluxes in other nanostructured electrodes, facilitating the design of optimized SC electrodes.

Notes

There are no conflicts to declare.

Acknowledgements

Wanli Gao acknowledges China Scholarship Council-Sorbonne University scholarship. The authors thank Ms. Françoise Pillier and Stéphanie Delbrel for the FEG-SEM measurements, and Mr. Cyrille Bazin for XRD measurements.

Supporting Information

MPE=F$\Delta m/\Delta q$ calculation from the EQCM data of the ZnO modified quartz resonators measured in 0.25M Na_2SO_4.

Corresponding authors:

*ozlem.sel@upmc.fr

*Hubert.perrot@upmc.fr

Notes and references

1. B. E. Conway, Kluwer Academic/Plenum, New York, 1999.

2. G. Wang, L. Zhang and J. Zhang, Chem. Soc. Rev., 2012, 41, 797-828.

3. J. R. Miller and P. Simon, Science, 2008, 321, 651-652.

4. T. Cottineau, M. Toupin, T. Delahaye, T. Brousse and D. Bélanger, Appl. Phys. A, 2006, 82, 599-606.

5. P. Simon and Y. Gogotsi, Nat. Mater., 2008, 7, 845-854.

6. V. Augustyn, P. Simon and B. Dunn, Energy Environ. Sci., 2014, 7, 1597.

7. T. Brezesinski, J. Wang, J. Polleux, B. Dunn and S. H. Tolbert, J. Am. Chem. Soc., 2009, 131, 1802-1809.

8. J. Shen, T. Li, W. Huang, Y. Long, N. Li and M. Ye, Electrochim. Acta, 2013, 95, 155-161.

9. X. Long, Z. Zeng, E. Guo, X. Shi, H. Zhou and X. Wang, J. Power Sources, 2016, 325, 264-272.

10. J. Bae, M. K. Song, Y. J. Park, J. M. Kim, M. Liu and Z. L. Wang, Angew. Chem. Int. Ed., 2011, 50, 1683-1687.

11. D.-W. Wang, F. Li and H.-M. Cheng, J. Power Sources, 2008, 185, 1563-1568.

12. B. R. Sankapal, H. B. Gajare, S. S. Karade, R. R. Salunkhe and D. P. Dubal, Electrochim. Acta, 2016, 192, 377-384.

13. P. H. Yang, X. Xiao, Y. Z. Li, Y. Ding, P. F. Qiang, X. H. Tan, W. J. Mai, Z. Y. Lin, W. Z. Wu, T. Q. Li, H. Y. Jin, P. Y. Liu, J. Zhou, C. P. Wong and Z. L. Wang, ACS Nano, 2013, 7, 2617-2626.

14. Y. B. He, G. R. Li, Z. L. Wang, C. Y. Su and Y. X. Tong, Energy Environ. Sci., 2011, 4, 1288-1292.

15. B. N. Illy, B. Ingham, M. F. Toney, I. Nandhakumar and M. P. Ryan, Langmuir, 2014, 30, 14079-14085.

16. A. Pruna, Q. Shao, M. Kamruzzaman, J. A. Zapien and A. Ruotolo, Electrochim. Acta, 2016, 187, 517-524.

17. Y.-L. Chen, Z.-A. Hu, Y.-Q. Chang, H.-W. Wang, Z.-Y. Zhang, Y.-Y. Yang and H.-Y. Wu, J. Phys. Chem. C, 2011, 115, 2563-2571.

18. A. R. Hillman, I. Efimov and M. Skompska, Faraday Discuss., 2002, 121, 423-439.

19. M. D. Levi, L. Daikhin, D. Aurbach and V. Presser, Electrochem. Commun., 2016, 67, 16-21.

20. S. Bruckenstein, K. Brzezinska and A. R. Hillman, Electrochim. Acta, 2000, 45, 3801-3811.

21. M. D. Levi, G. Salitra, N. Levy, D. Aurbach and J. Maier, Nat. Mater., 2009, 8, 872-875.

22. Z. Lin, P.-L. Taberna and P. Simon, Curr. Opin. Electrochem., 2018, DOI:10.1016/j.coelec.2018.03.004, https://doi.org/10.1016/j.coelec.2018.1003.1004.

23. N. Shpigel, M. D. Levi, S. Sigalov, D. Aurbach, L. Daikhin and V. Presser, J. Phys. Condens. Matter, 2016, 28, 114001.

24. V. Dargel, N. Shpigel, S. Sigalov, P. Nayak, M. D. Levi, L. Daikhin and D. Aurbach, Nat. Commun., 2017, 8, 1389.

25. M. D. Levi and D. Aurbach, Electrochim. Acta, 1999, 45, 167-185.

26. C. Gabrielli, J. J. Garcia-Jareno, M. Keddam, H. Perrot and F. Vicente, J. Phys. Chem. B, 2002, 106, 3192-3201.

27. F. Escobar-Teran, A. Arnau, J. V. Garcia, Y. Jiménez, H. Perrot and O. Sel, Electrochem. Commun., 2016, 70, 73-77.

28. H. Goubaa, F. Escobar-Teran, I. Ressam, W. Gao, A. El Kadib, I. T. Lucas, M. Raihane, M. Lahcini, H. Perrot and O. Sel, J. Phys. Chem. C, 2017, 121, 9370-9380.

29. C. R. Arias, C. Debiemme-Chouvy, C. Gabrielli, C. Laberty-Robert, A. Pailleret, H. Perrot and O. Sel, J. Phys. Chem. C, 2014, 118, 26551-26559.

30. G. Sauerbrey, Z. Phys., 1959, 155, 206-210.

31. K. Bizet, C. Gabrielli and H. Perrot, Appl. Biochem. Biotechnol., 2000, 89, 139-149.

32. W. Gao, O. Sel and H. Perrot, Electrochim. Acta, 2017, 233, 262-273.

33. X. Dong, Y. Cao, J. Wang, M. B. Chan-Park, L. Wang, W. Huang and P. Chen, RSC Adv., 2012, 2, 4364.

34. J. Wang, Z. Gao, Z. S. Li, B. Wang, Y. X. Yan, Q. Liu, T. Mann, M. L. Zhang and Z. H. Jiang, J. Solid State Chem., 2011, 184, 1421-1427.

35. C. Gabrielli, J. J. Garcia-Jareño and H. Perrot, Electrochim. Acta, 2001, 46, 4095-4103.

36. H. M. French, M. J. Henderson, A. R. Hillman, E. Vieil, *Solid State Ionics*, 2002, *150*, 27-37.

37. H. M. French, M. J. Henderson, A. R. Hillman, E. Vieil, *J. Electroanal. Chem.,* 2001, *500*, 192-207.

38. M. Gonsalves, A. R. Hillman *J. Electroanal. Chem.,* 1998, *454*, 183-202.

39. H. Y. Lee and J. B. Goodenough, J. Solid State Chem., 1999, 144, 220-223.

40. S.-C. Pang, M. A. Anderson and T. W. Chapman, J. Electrochem. Soc., 2000, 147, 444-450.

41. M. Toupin, T. Brousse and D. Bélanger, Chem. Mater., 2004, 16, 3184-3190.

FIGURES

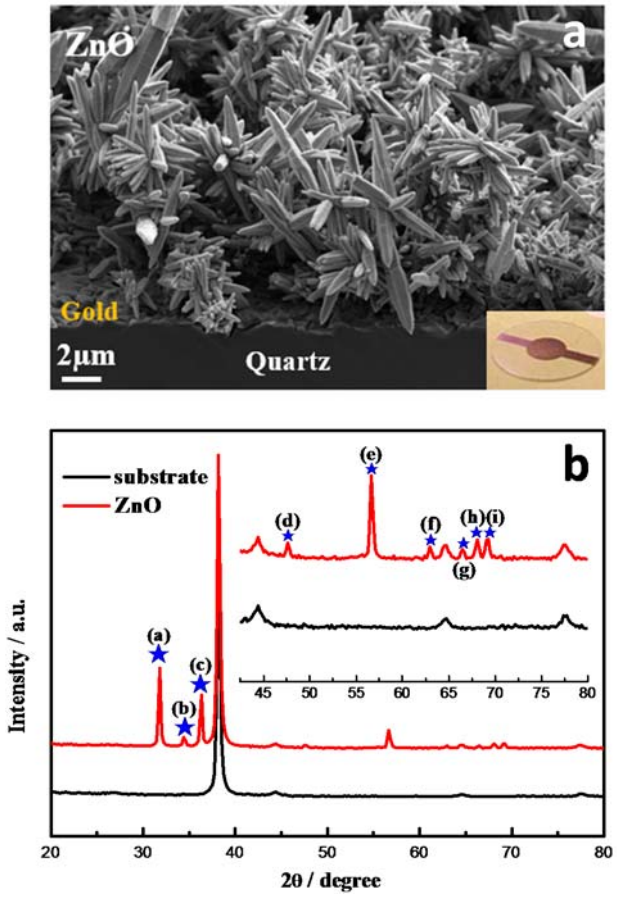

Fig. 1 (a) FEG-SEM image and **(b)** XRD spectra of ZnO nanostructures hydrothermally synthesized on the gold electrode of the quartz resonator. The peaks centered at 2θ = 32°, 34°, 36°, 47°, 56°, 63°, 66°, 68° and 69° correspond to the lattice planes (100), (002), (101), (102), (110), (103), (200), (112) and (201), respectively. The inset in (b) is the magnification between 2θ = 42.5° and 80°.

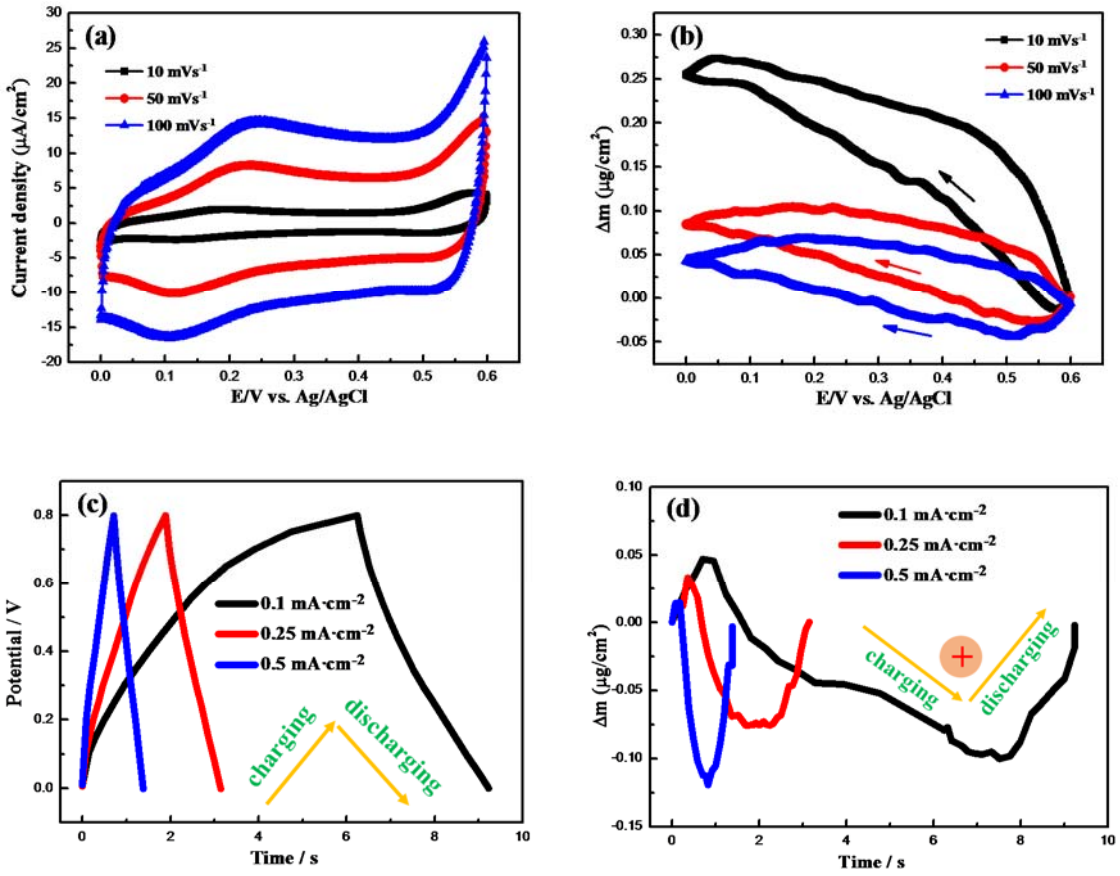

Fig. 2 Cyclic voltammetry **(a)** and galvanostatic charge/discharge **(c)** measurements of ZnO electrode on the gold electrode of the quartz resonator with the corresponding mass variations of the electrode **(b and d)** measured in 0.25 M Na_2SO_4.

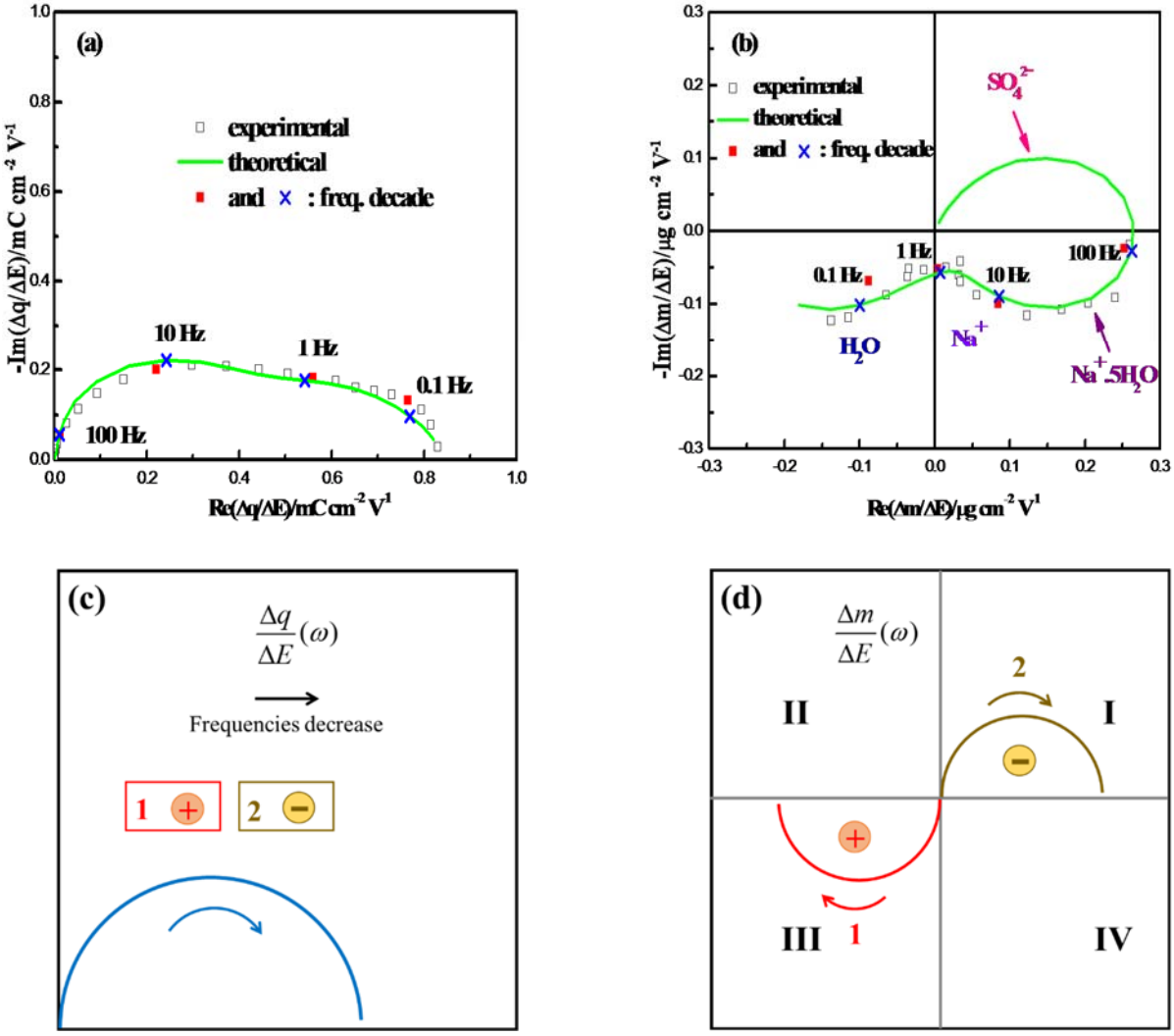

Fig. 3 $\Delta q/\Delta E(\omega)$ (a) and $\Delta m/\Delta E(\omega)$ (b) Transfer Functions (TFs) at 0.3V *vs.* Ag/AgCl. Schematic representation of the TFs for $\Delta q/\Delta E(\omega)$ (c) and $\Delta m/\Delta E(\omega)$ (d). The following parameters were used in the fitting of the experimental data: K_i (kinetics of transfer, in $cm \cdot s^{-1}$), G_i (the inverse of the transfer resistance, in $mol \cdot s^{-1} \cdot cm^{-2} \cdot V^{-1}$): Kc1: 0.0088, Gc1: 2.375×10^{-7}; Kc2: 2.199×10^{-4}, Gc2: 9.456×10^{-9}; Ks: 3.77×10^{-5}, Gs: 4.524×10^{-9}; Ka: 0.06, Ga: -2.149×10^{-6}. C_1: $Na^+.5H_2O$ (113 $g.mol^{-1}$), C_2: Na^+ (23 $g.mol^{-1}$), S: H_2O (18 $g.mol^{-1}$) and A: SO_4^{2-} (96 $g.mol^{-1}$).

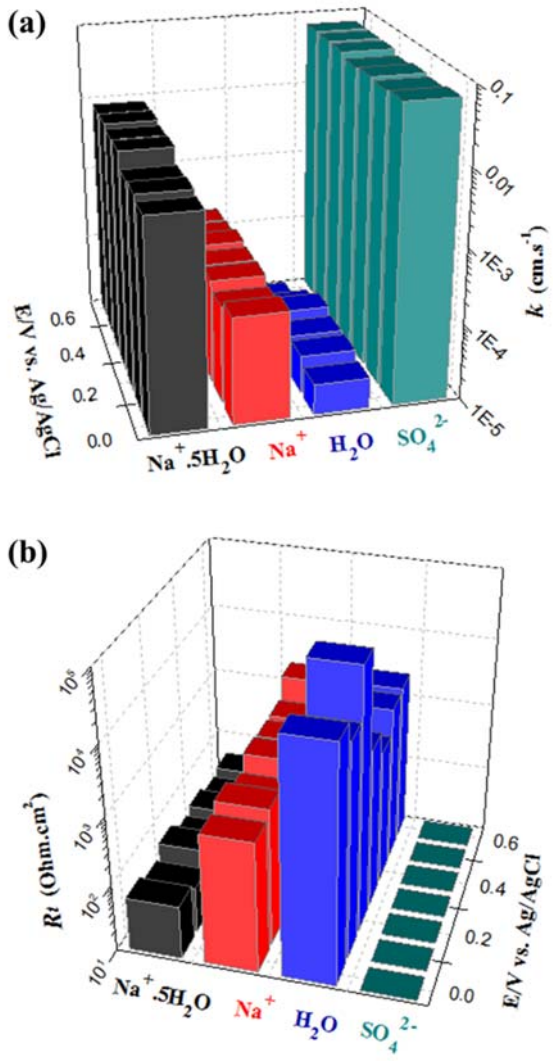

Fig. 4 Transfer kinetics, K_i ($cm \cdot s^{-1}$) (a) and corresponding transfer resistances, Rt_i ($\Omega \cdot cm^2$) (b) for each species participating in charge balance.

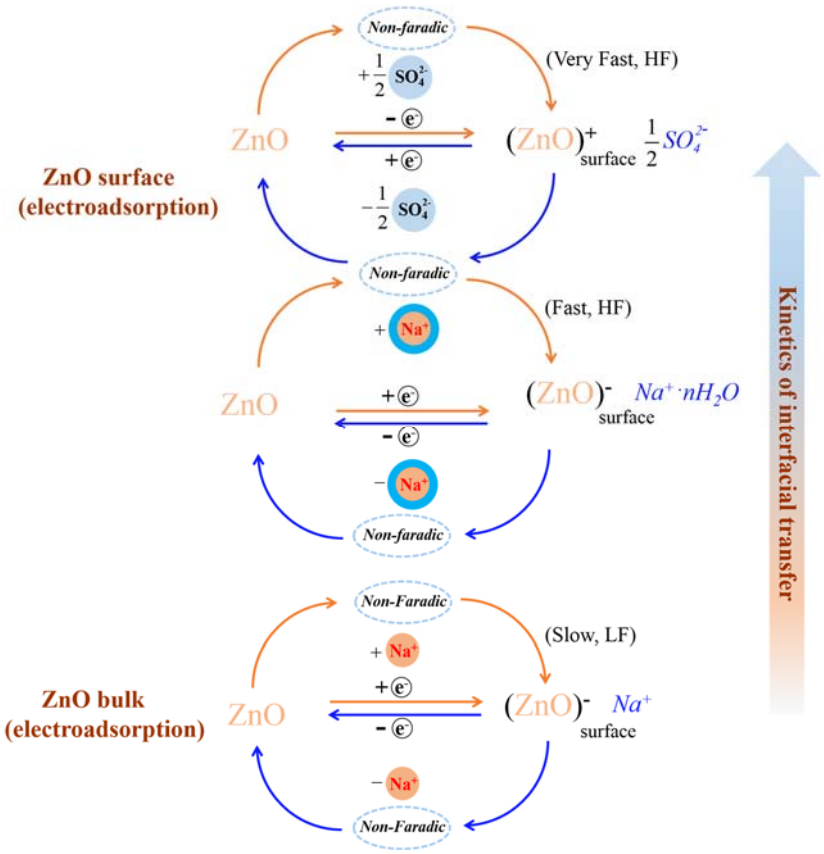

Fig.5 A schematic presentation of ions participating in the charge balance, where cations with blue shell (1st step) represent the hydrated cation, i.e., $Na^{+}.nH_2O$ (n=5).

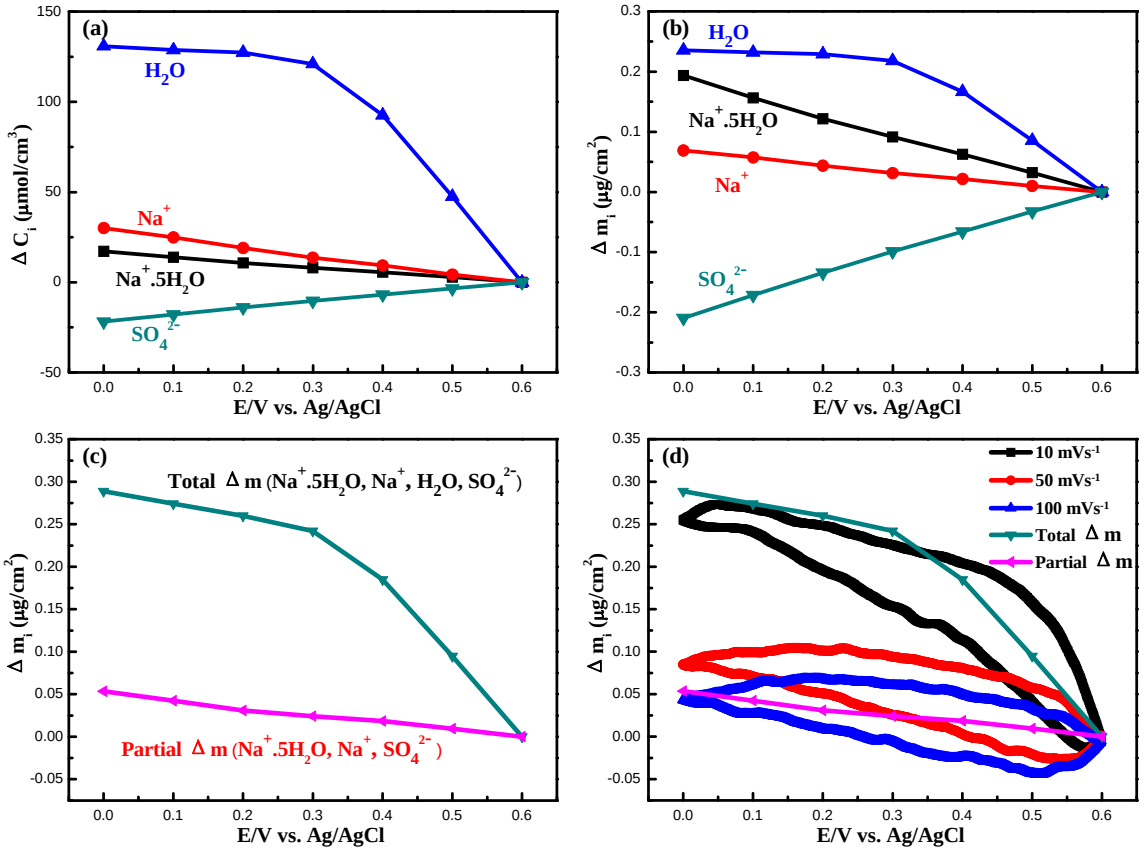

Fig. 6 Relative concentration change (a) and the corresponding mass change (b) of each species as a function of potential; mass variation (Total and Partial Δ*m*) reconstructed from *ac*-electrogravimetry (c) and the comparison of mass variation between *ac*-electrogravimetry and EQCM (d).

Supporting Information

Tracking interfacial charge transfer behavior of hydrothermally synthesized ZnO nanostructures via complementary electrogravimetric methods

Wanli Gao[a], Hubert Perrot [a,*], Ozlem Sel[a,*]

[a] Sorbonne Université, CNRS, UMR 8235, LISE, F-75005, Paris, France.

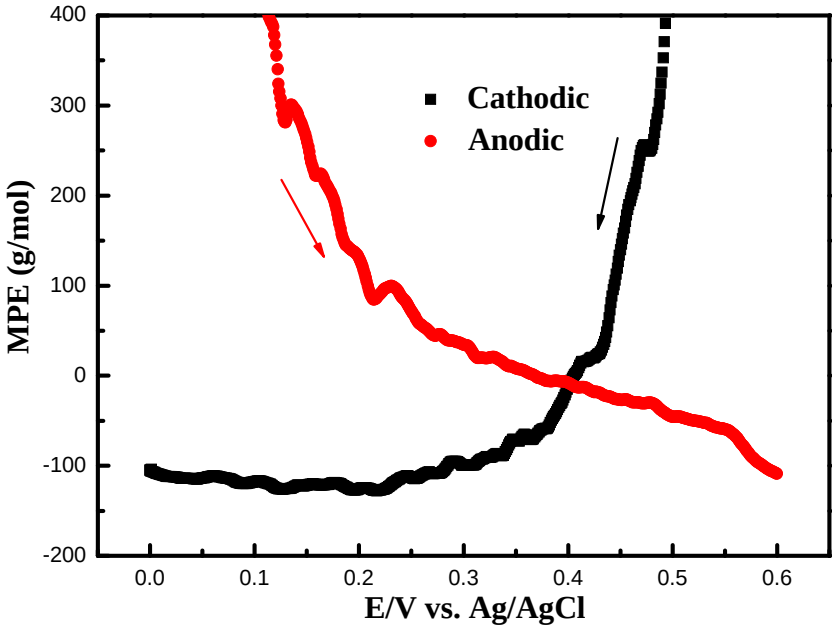

Fig. S1 MPE calculated from CV curve at a scan rate of 50 mV/s.

E-mail address: hubert.perrot@upmc.fr (H. Perrot).
E-mail address: ozlem.sel@upmc.fr (O. Sel).